Modelling of radiation-induced segregation at grain boundaries in austenitic stainless steels

Norihito Sakaguchi
Hokkaido University, Japan

Abstract

A model for radiation-induced segregation (RIS) at grain boundaries was developed based on the rate equations including the inverse-Kirakendall fluxes and the interactions between point defects and minor alloying elements. The dependencies of irradiation temperature and damage rate on the RIS were theoretically predicted by the present model. The effect of the additional minor alloying elements on the RIS was also examined. The multi-component RIS model, which was including the contribution of the minor alloying elements, successfully reproduced the RIS behaviour in neutron irradiated type 304L and 316L austenitic stainless steels.

Introduction

Solute redistribution in a concentrated alloy under irradiation occurs due to the preferential interaction between the solute atoms and excess point defects migrating toward sinks, such as surface or grain boundaries. In the austenitic stainless steels type 304 and 316, which are used as a light-water reactor core materials, radiation-induced segregation (RIS) near the grain boundaries significantly degrades their mechanical chemical properties. The seriousness of this problem has been considered as irradiation-assisted stress corrosion cracking (IASCC) induced by the RIS because of the depletion of chromium atoms near grain boundaries. It is thus important to investigate the mechanism for retardation of radiation-induced solute redistribution near the grain boundaries.

In the present paper, the defect kinetic rate equations were used to evaluate the RIS behaviour around the grain boundaries in austenitic stainless steels. To clarify the validity of the present model and a set of physical parameters, the calculated results were compared to some experimental results obtained by the electron and neutron irradiation experiments.

Simulation Method

Simultaneous solutions to rate equations describe solute redistribution induced by vacancies and interstitials fluxes to grain boundaries and by solute interactions with those defect fluxes. The present RIS model is based on a simple model for ternary Fe-Cr-Ni system described by Marwick et al. (Marwick, 1983). The composition-dependent diffusion coefficients introduced by Allen et al. (Allen, 1997) is not considered in the present model. Finite difference method and the LSODE subroutine (LSODE, 1980) have been used to solve the rate equations.

Continuity equations for point defects and major alloying elements

The approach is to solve the couple diffusion equations for vacancies, interstitials and alloying elements to obtain the terms coupling the defect and solute fluxes. The continuity equations are

$$\frac{\partial C_v}{\partial t} = -\frac{\partial J_v}{\partial x} + \eta G_{dpa} - R_{vi} D_i C_v C_i - S_v D_v (C_v - C_v^{th}) \quad (1)$$

$$\frac{\partial C_i}{\partial t} = -\frac{\partial J_i}{\partial x} + \eta G_{dpa} - R_{vi} D_i C_v C_i - S_i D_i C_i \quad (2)$$

$$\frac{\partial C_k}{\partial t} = -\frac{\partial J_k}{\partial x} \quad (k = Fe, Cr, Ni) \quad (3)$$

where C_v and C_i are the concentrations of vacancy and interstitial, C_k is the concentration of alloying element k, η is the damage efficiency, G_{dpa} is the displacement production rate of point defects, R_{vi} is the mutual recombination coefficient, D_v and D_i are the diffusivities of vacancy and interstitial, S_v and S_i are the internal sink strength for vacancy and interstitial, and C_v^{th} is the thermal equilibrium concentration of vacancy. The fluxes, J_v, J_i and J_k, are written by

$$J_v = -D_v \frac{\partial C_v}{\partial x} + C_v \sum_k d_k^v \frac{\partial C_k}{\partial x} \quad (4)$$

$$J_i = -D_i \frac{\partial C_i}{\partial x} - C_i \sum_k d_k^i \frac{\partial C_k}{\partial x} \quad (5)$$

$$J_k = -D_k \frac{\partial C_k}{\partial x} + C_k \left(d_k^v \frac{\partial C_v}{\partial x} - d_k^i \frac{\partial C_i}{\partial x} \right) \quad (6)$$

where D_k is the diffusivity of alloying element k, d_k^v and d_k^i are the partial diffusion coefficients of solutes by vacancies and by interstitials. In the flux equations (4) and (5) for point defects, last term shows the contribution of the Kirkendall flux due to the concentration gradient of the solute atoms. In the flux equation (6) for alloying elements, the last two terms indicate the inverse-Kirkendall fluxes due to the concentration gradients of vacancies and interstitials respectively. Of main interest are the coupling parameters, d_k^v and d_k^i, determined by

$$d_k^v = a_0^2 \nu_k^v \exp(-E_m^v / k_B T) \quad (7)$$

$$d_k^i = a_0^2 \nu_k^i \exp\left(-E_m^i / k_B T\right) \quad (8)$$

where ν_k^v and ν_k^i are the jump frequencies of vacancy and interstitial via the k-atom, a_0 is the lattice constant, E_m^v and E_m^i are the migration energies of the vacancy and interstitials, respectively. The diffusivities of point defects and the solute atoms are the given by

$$D_v = \sum_k d_k^v C_k \quad (9)$$

$$D_i = \sum_k d_k^i C_k \quad (10)$$

$$D_k = d_k^v C_v + d_k^i C_i \ . \quad (11)$$

Continuity equations for minor alloying elements

Considering the flux of minor alloying elements and the interaction with the point defects, a few additional parameters should be introduced to the continuity equations. Since the additives, silicon and phosphorous, are the undersized solute elements in austenitic stainless steels, they are thought to preferentially interact with interstitial atoms and form mixed-dumbbells (Sakaguchi, 2005). On the other hands, the minor alloying elements such as manganese and molybdenum are the oversized solutes in the austenitic stainless steels. These oversized elements only interacted with vacancies and formed additive-vacancy complexes ([Sakaguchi, 1999], [Hackett, 2009]).

For the undersized solute elements, we introduced a new coupling parameter in the flux equations (5) and (6). The flux equation is rewritten as

$$J_i = -D_i \frac{\partial C_i}{\partial x} - C_i \sum_k d_k^i \beta_k \frac{\partial C_k}{\partial x} \quad (12)$$

$$J_k = -D_k \frac{\partial C_k}{\partial x} + C_k \left(d_k^v \frac{\partial C_v}{\partial x} - d_k^i \beta_k \frac{\partial C_i}{\partial x} \right) . \quad (13)$$

The important parameter here is the coupling parameter between interstitial and solute atoms described by

$$\beta_k = \frac{C_k \exp(E_{k-i}^b / k_B T)}{\sum_m C_m \exp(E_{m-i}^b / k_B T)} \quad (14)$$

where $E_{k\text{-}i}^b$ is the binding energy between an interstitial atom and solute atom. This parameter provides the fraction of each solute element forming the mixed-dumbbell in all of the mixed-dumbbells, and the magnitude of β_k becomes large with increase in binding energy. Undersized-solute elements such as silicon and phosphorus, which are expected to easily form a mixed-dumbbell, are thought to have larger β that those of the other solute elements. In the present calculation, the binding energies were selected to be positive values for silicon and phosphorus, and zero for the other alloying elements. The diffusivities of interstitials and solute atoms are also rewritten as

$$D_i = \sum_k d_k^i \beta_k C_k \quad (15)$$

$$D_k = d_k^v C_v + d_k^i \beta_k C_i \ . \quad (16)$$

For the oversized solutes, the continuity equations for the point defects and oversized solutes M are rewritten as

$$\frac{\partial C_v}{\partial t} = -\frac{\partial J_v}{\partial x} + G_{dpa} - R_{vi} D_i C_v C_i - S_v D_v (C_v - C_v^{th}) - K_{Mv} D_v C_M C_v + K_{Mv}^r D_v C_{Mv} \quad (17)$$

$$\frac{\partial C_i}{\partial t} = -\frac{\partial J_i}{\partial x} + G_{dpa} - R_{vi} D_i C_v C_i - S_i D_i C_i - R_{vi} D_i C_i C_{Mv} \quad (18)$$

$$\frac{\partial C_M}{\partial t} = -\frac{\partial J_M}{\partial x} - K_{Mv} D_v C_M C_v + K_{Mv}^r D_v C_{Mv} + R_{vi} D_i C_i C_{Mv} \quad (19)$$

where K_{Mv} is the reaction coefficient between a vacancy and solute atom, $K_{Mv}{}^{r}$ is the thermal dissociation rate of the vacancy-solute complex, and C_{Mv} is the concentration of the vacancy-solute complexes. The dissociation rate of the complex is determined by

$$K_{Mv}^{r} = Z_{Mv} \exp\left(-E_{M-v}^{b}/k_B T\right) \tag{20}$$

where $E_{M\text{-}v}{}^{b}$ is the binding energy between a vacancy and solute atom and Z_{Mv} is the geometrical coordination number of the complexes. The binding energies were selected to be positive values for manganese, molybdenum and other oversized additives, and zero for the other alloying elements. The migration of the vacancy-solute complexes was neglected in the present calculation and the reaction rate equation for the complexes is described by

$$\frac{\partial C_{Mv}}{\partial t} = K_{Mv} D_v C_M C_v - K_{Mv}^{r} D_v C_{Mv} - R_{vi} D_i C_i C_{Mv} \ . \tag{21}$$

Boundary condition at grain boundaries

The continuity equations were evaluated as functions of the one-dimensional coordinate perpendicular to the grain boundary and of the irradiation time. The boundary conditions for the alloying elements are zero flux at the grain boundary and at the center of a grain. Similarly, the defect fluxes are assumed to be zero at the center of a grain, but the grain boundary concentrations are fixed at the equilibrium concentration for vacancies and zero for interstitial atoms , so-called “perfect sink condition”, described by

$$C_v|_{GB} = C_v^{th} \tag{22}$$

$$C_i|_{GB} = 0 \ . \tag{23}$$

However, the “perfect sink condition” sometimes overestimates the segregation behaviour at the small angle boundaries and coincidence site lattice (CSL) boundaries. These boundaries do not act as a perfect sink, thus we additionally defined the sink strength of the grain boundary and equations (1) and (2) are rewritten as

$$\left.\frac{\partial C_v}{\partial t}\right|_{GB} = -\frac{\partial J_v}{\partial x} + G_{dpa} - R_{vi} D_i C_v C_i - S_v D_v (C_v - C_v^{th}) - S_{GB} D_v (C_v - C_v^{th}) \tag{24}$$

$$\left.\frac{\partial C_i}{\partial t}\right|_{GB} = -\frac{\partial J_i}{\partial x} + G_{dpa} - R_{vi} D_i C_v C_i - S_i D_i C_i - S_{GB} D_i C_i \tag{25}$$

where S_{GB} is the sink strength of the grain boundary, which is a function of the misorientation angle and Σ value ([Watanabe, 2000], [Sakaguchi, 2004]).

Effect of probe size on TEM/EDX measurement

Comparing the calculated concentration profiles to the experimental profiles obtained by the TEM/EDX, it is important to consider the averaging effect due to the finite size probe (about 1 nm in FEG-TEM) in the EDX analysis (Watanabe, 1995). The one-dimensional calculated concentration profile is convoluted by the normalized two-dimensional Gaussian function (see figure 1), which is expressed by

$$C^{EDX}(x) = \frac{\sqrt{a/\pi}}{1-\exp(-aR^2)} \int_{-R}^{R} \exp(-ar^2) \times \mathrm{Erf}\left[\sqrt{a(R^2 - r^2)}\right] \times C(x-r)dr \tag{26}$$

where C^{EDX} is the averaged concentration profile, i.e., series of concentrations obtained by the TEM/EDX analysis, R is the probe radius, and a is the deviation constant described as

$$a = \frac{1}{2R^2} \ . \tag{27}$$

This procedure is of importance for simulating the actual profile data taken by the TEM/EDX.

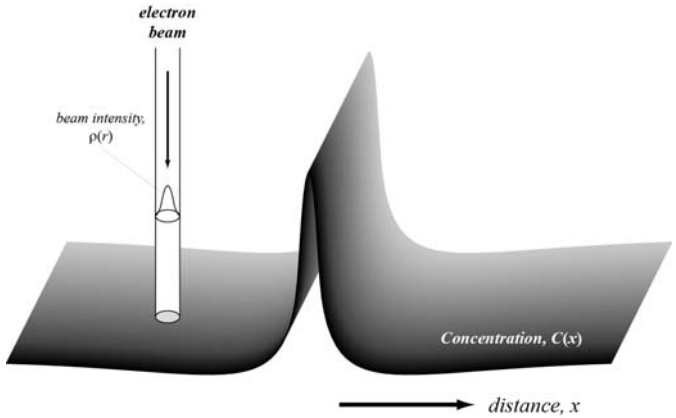

Figure 1: Schematic illustration of one-dimensional concentration profile and electron probe intensity.

Determination of physical parameters

The material constants used in the present calculations are listed in table 1. The solute-defect interactions are ignored for the major alloying elements (Fe, Cr and Ni). It is assumed that the interstitial only interacts with the undersized minor alloying elements (Si, P), whereas the vacancy forms the vacancy-solute complex with the oversized minor alloying elements (Mn, Mo).

Vacancy migration energy	E_m^v	1.05eV
Fe-vacancy jump frequency	ν_{Fe}^v	$5.0e13s^{-1}$
Cr-vacancy jump frequency	ν_{Cr}^v	$8.0e13s^{-1}$
Ni-vacancy jump frequency	ν_{Ni}^v	$2.5e13s^{-1}$
Mn-vacancy jump frequency	ν_{Mn}^v	$1.0e14s^{-1}$
Mo-vacancy jump frequency	ν_{Mo}^v	$1.2e14s^{-1}$
Si-vacancy jump frequency	ν_{Si}^v	$5.0e14s^{-1}$
P-vacancy jump frequency	ν_P^v	$5.0e14s^{-1}$
Interstitial migration energy	E_m^i	0.85eV
Interstitial jump frequency	ν^i	$5.0e12s^{-1}$
Si-interstitial dumbbell migration energy	ν_{Si}^i	1.2eV
P-interstitial dumbbell migration energy	ν_P^i	1.4eV
Mn-vacancy binding energy	$E_{Mn\text{-}v}^b$	0.2eV
Mo-vacancy binding energy	$E_{Mo\text{-}v}^b$	0.4eV
Si-interstitial dumbbell binding energy	$E_{Si\text{-}i}^b$	0.5eV
P-interstitial dumbbell binding energy	$E_{P\text{-}i}^b$	0.7eV
Mutual recombination coefficient	R_{vi}	$500/a_0^2$
Vacancy-solute reaction coefficient	K_{Mv}	$30/a_0^2$
Vacancy-solute dissociation coefficient	Z_{Mv}	$14/a_0^2$
Point defect production rate	η	
electron irradiation		1.0
neutron irradiation		0.03
Internal sink strength for vacancy	S_v	
electron irradiation		$1.0e14m^{-2}$
neutron irradiation		$1.0e15m^{-2}$
Internal sink strength for interstitial	S_i	1.1 Sv

Table 1: Main parameters used in the present calculations.

Calculations

RIS behaviour in Fe-Cr-Ni ternary alloy

A typical theoretical prediction of solute segregation near a random grain boundary in Fe-15Cr-20Ni alloy after electron irradiation to 1 dpa ant 673 K is shown in figure 2. Experimental data also are also plotted in the figure. Irradiation-induced nickel enrichment and chromium depletion at the grain boundary were quantitatively reproduced by the present RIS model. Figure 3 shows the temperature dependencies of nickel and chromium concentrations at the random grain boundaries after electron irradiation to 1 dpa. Both the theoretical and experimental data suggest that the peak temperature of the RIS is about 800 K in the present irradiation condition. This peak temperature is depending on the displacement production rate of point defects. To clarify this, calculated three-dimensional plots of the RIS at a grain boundary after irradiation to 0.1 dpa are shown in figure 4. The maxima in nickel and minima in chromium by the RIS with temperature change are clearly seen, and their shift with the damage rate is manifest. We can see that the peak temperature of the RIS falls in decreases of the damage rate but the magnitude of the RIS increases. Figure 5 shows a schematic drawing of the relationship the RIS between the temperature and the damage rate. The RIS at a grain boundary is suppressed at higher temperature because of the back diffusion of solute elements that counters segregation driven by the irradiation; on the other hands, the suppression of the RIS also occurs at lower temperature because the short-range mutual recombination of the vacancies and interstitials becomes dominant. Hence, a maximum of the RIS is expected at intermediate temperature and the higher damage rate elevates the peak temperature of the RIS.

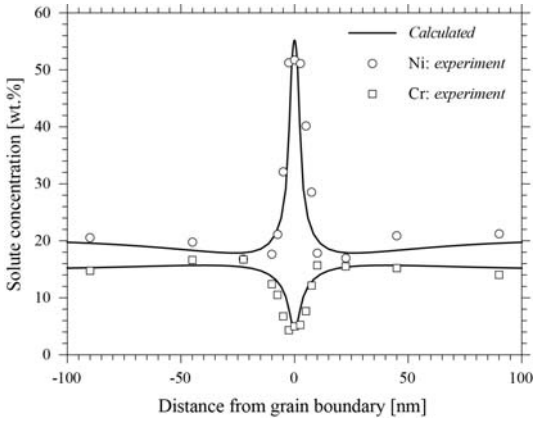

Figure 2: Solute concentration profiles near a random grain boundary after electron irradiation to 1 dpa at 673 K in Fe-15Cr-20Ni ternary alloy.

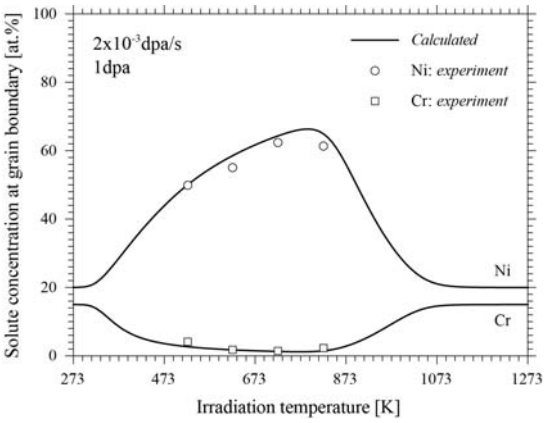

Figure 3: Temperature dependence of RIS at random grain boundaries after electron irradiation to 1 dpa at 2×10^{-3} dpa/s.

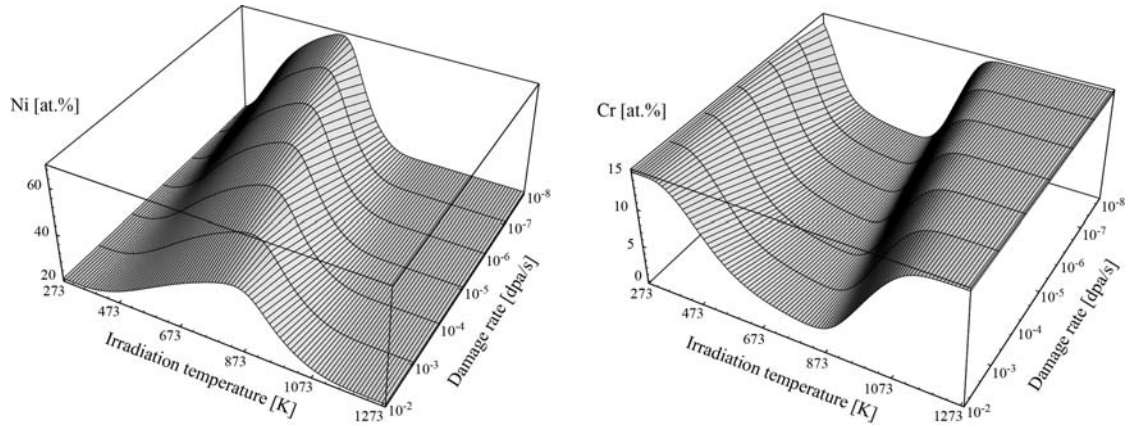

Figure 4: Three-dimensional plots of temperature and damage rate dependence of RIS at a grain boundary in Fe-15Cr-20Ni alloy after irradiation to 0.1 dpa.

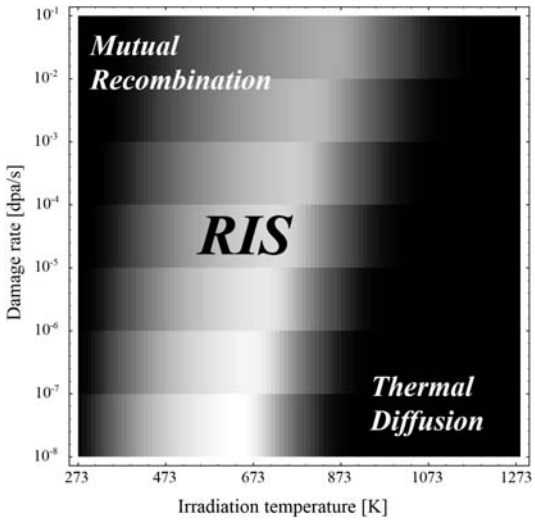

Figure 5: Schematic drawing of the relationship the RIS between the temperature and the damage rate.

Effect of additional minor alloying element on RIS

In order to overview the effect of addition of a minor alloying element, a typical theoretical prediction of the temperature dependence on the RIS at a grain boundary in Fe-15Cr-20Ni with or without the additional element after irradiation to 3dpa is shown in figure 6. In this calculation, we assumed that the additional element only interacted with vacancies, and the diffusion of the additional element was neglected. The concentration of the additional element and the additive-vacancy binding energy were 0.5 at.% and 0.5 eV, respectively. It was predicted that the amount of segregation at the grain boundary decreased in the presence of the additional element at elevated temperature. Here we divide the temperature dependence of the RIS in three stages.

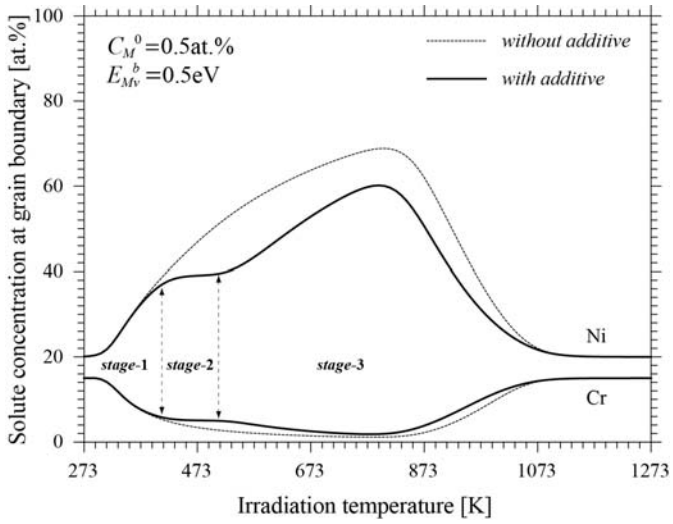

Figure 6: Temperature dependence of RIS in Fe-15Cr-20Ni alloy with or without oversized additional element at grain boundary after electron irradiation to 3 dpa.

1. At the temperatures below 400 K, the RIS is not affected by the additional minor element which interacts with the vacancies (stage-1). At this stage, the mobility of the vacancies is too small to form the additive-vacancy complexes. Almost of the vacancies annihilates due to the mutual recombination of the neighbouring interstitial atoms.
2. Above that temperature, the temperature region in which the amount of the RIS is kept constant appears (stage-2). Almost of the vacancies are trapped by the additional elements at this temperature regime, and the dominant defect reaction is the recombination between the additive-vacancy complexes and the interstitial atoms. In the present situation, radiation-enhanced diffusivities of the alloying elements do not depend on the temperature.

3. Further increase of temperature, the amount RIS increases with the temperature (stage-3), but it decreases than that in the Fe-Cr-Ni ternary alloy. At this stage, the dissociation of the additive-vacancy complexes occurs and the some parts of the free-vacancies diffuse again to the grain boundary and annihilate there. The appearance activation energy of the vacancy diffusion equals to the sum of the vacancy migration energy and the additive-vacancy binding energy.

The additive concentration dependencies on solute segregation at a grain boundary after irradiation to 3 dpa are shown in figure 7. The binding energy between the additive and vacancies used was 0.5 eV. The amount of the RIS decreased in increases of the additive concentration at the temperature ranges of the stage-2 and stage-3. The magnitude of the decrement gradually became saturated at higher additive concentrations and the transient temperatures of each stage ($T_{stage1\text{-}2}$ and $T_{stage2\text{-}3}$) did not depend on the additive concentration. Figure 8 shows the additive-vacancy binding energy dependencies on solute segregation at a grain boundary. The concentration of the additional element used was 0.5 at.%. It was also predicted that the amount of the RIS decreased in increases of the additive-vacancy binding energy at the temperature ranges of the stage-2 and stage-3. The transient temperature from stage-1 to stage-2 ($T_{stage1\text{-}2}$) did not depend on the additive-vacancy binding energy; however, the transient temperature from stage-2 to stage-3 ($T_{stage2\text{-}3}$) shifted to higher temperature as increasing of the binding energy and the RIS was strongly suppressed at the temperatures corresponding to the stage-3. It was expected that the additive-vacancy binding energy was correlated with the size factor of oversized additional elements ([Sakaguchi, 1999], [Hackett, 2009]). For examples, addition of hafnium and zirconium, which were the oversized additional elements with large additive-vacancy binding energy (~ 1 eV), to type 316L stainless steels nearly suppressed the RIS on the grain boundaries at the stage-3 temperature regime (Kato, 1992).

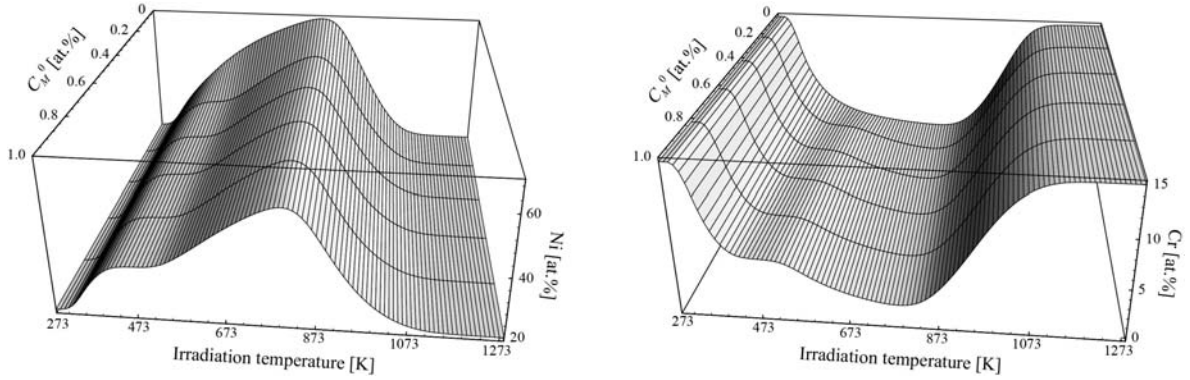

Figure 7: Three-dimensional plots of temperature and additive concentration dependence of RIS at a grain boundary in Fe-15Cr-20Ni alloy with oversized additional alloying elements.

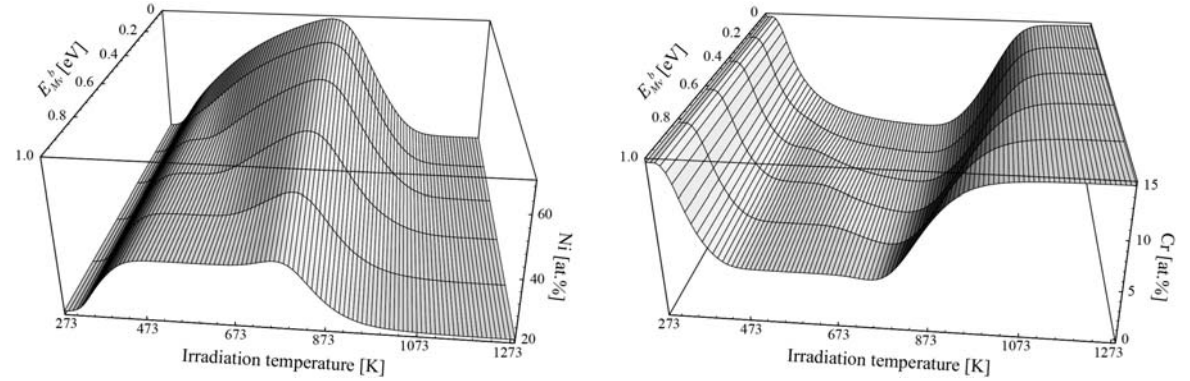

Figure 8: Three-dimensional plots of temperature and additive-vacancy binding energy dependence of RIS at a grain boundary in Fe-15Cr-20Ni alloy with oversized additional alloying elements.

The effect of the undersized alloying elements on the RIS shows same tendency caused by the oversized additional elements. The undersized elements preferentially interact with the interstitial atoms and form the mixed-dumbbells. In general, the migration energy of the mixed-dumbbell is higher than that the migration energy of the self-interstitials, so that the appearance activation energy of the interstitial diffusion increases. Figure 9 shows the temperature dependence on the RIS at a grain boundary with or without the undersized additional element after irradiation to 3dpa. The migration of the mixed-

dumbbells was neglected in the present calculation. The amount of the RIS decreased in the presence of the undersized additional element at elevated temperature and same stages appeared in the temperature dependence of the RIS. It has been reported that the addition of the undersized additional elements such as silicon and phosphorous drastically suppressed the RIS at the grain boundaries (Sakaguchi, 2005). It was suggested that the phosphorous suppressed the RIS more effectively because of a strong interaction with the interstitial atoms.

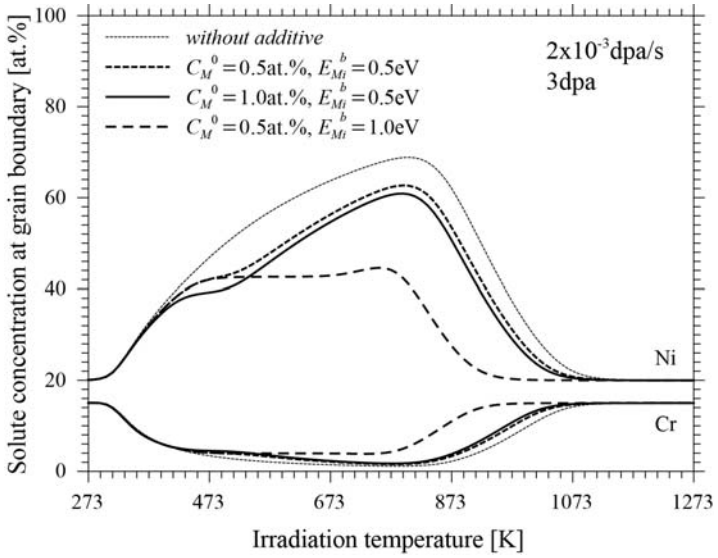

Figure 9: Temperature dependence of RIS in Fe-15Cr-20Ni alloy with or without undersized additional element at grain boundary after electron irradiation to 3 dpa.

Prediction by multi-component RIS model

It was reconfirmed that the addition of the minor alloying elements strongly influenced to the RIS behaviour of the major alloying elements like chromium. The theoretical prediction using the multi-component RIS model is needed to estimate quantitatively the RIS behaviour in neutron irradiated materials. Figure 10 shows the calculated concentration profiles of nickel, chromium and silicon in Fe-21Cr-8Ni-1Si-0.05P-1.5Mn alloy after irradiation to 1 dpa at 561 K. The experimental data was obtained by the neutron irradiated type 304L stainless steel. In the present parameter set (see table 1), silicon and phosphorous interact with the interstitial atoms, whereas the manganese acts as the vacancy trapping element. Fairly good agreement between the calculated and experimental concentration profiles was achieved. It is notice that the Fe-

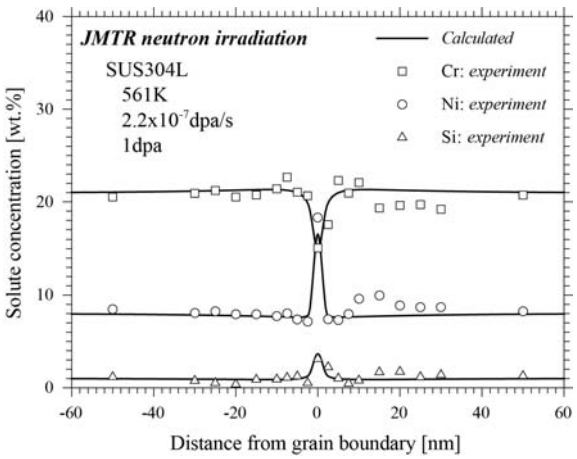

Figure 10: Concentration profiles of nickel, chromium and silicon near grain boundary in 304L stainless steel after neutron irradiation to 1 dpa.

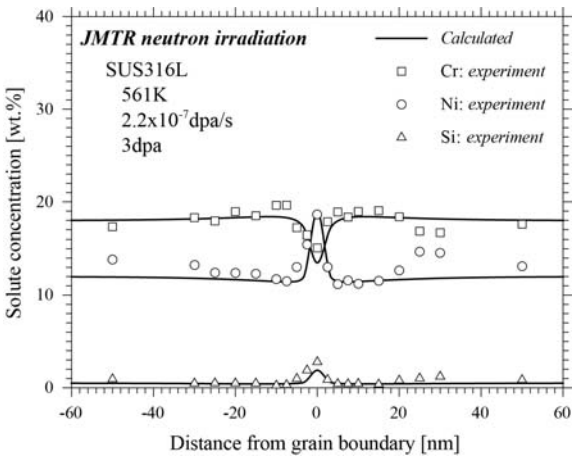

Figure 11: Concentration profiles of nickel, chromium and silicon near grain boundary in 316L stainless steel after neutron irradiation to 3 dpa.

Cr-Ni ternary RIS model failed to reproduce the solute profiles, it overestimated the RIS at the grain boundary. In figure 11, the concentration profiles of nickel, chromium and silicon in neutron irradiated type 316L stainless steel are plotted with the theoretical values. The irradiation dose and the temperature were 3 dpa and 561 K, respectively. In the theoretical prediction, we considered the Fe-18Cr-12Ni-0.5Si-0.05P-1.5Mn-2.5Mo alloy system as a model for the 316L stainless steel. Molybdenum is assumed to be the vacancy trapping element as same as the manganese. The binding energy between the molybdenum and vacancy used (0.4 eV) was higher than that of the manganese (0.2 eV). Even though the irradiation dose was higher than the former case, the amount of the RIS at the grain boundary was less than that in the type 304 stainless steel. This reflects that the molybdenum acts as stronger vacancy trapping element than the manganese, as assumed in the calculations.

Conclusion

We proposed a model for radiation-induced segregation (RIS) at grain boundaries based on the rate equations including the inverse-Kirakendall fluxes and the interactions between point defects and minor alloying elements. The relationship between irradiation temperature, damage rate and the RIS on the grain boundaries were theoretically predicted by the present model. It was confirmed that the peak temperature of the RIS falls in decreases of the damage rate but the magnitude of the RIS increases. It was revealed that the RIS was significantly affected by the additional minor alloying elements which interacted with the vacancies or interstitials. The multi-component RIS model can successfully reproduce the RIS behaviour in neutron irradiated type 304L and 316L austenitic stainless steels.

References

[Allen, 1997] T.R. Allen, G.S. Was, E.A. Kenik, J. Nucl. Mater. 244 (1997) 278.

[Hackett, 2009] M.J. Hackett, R. Najafabadi, G.S. Was, J. Nucl. Mater. 389 (2009) 279.

[Kato, 1992] T. Kato, H. Takahashi, M. Izumiya, J. Nucl. Mater. 189 (1992) 167.

[LSODE, 1980] A.C. Hindmarsh, LSODE: Livermore Solver for Ordinary Differential Equations, Lowrence Livermore National Laboratory, (1980).

[Marwick, 1983] A.D. Marwick, R.C. Piller and M.E. Horton, AERE-R 10895, (1983).

[Sakaguchi, 1999] N. Sakaguchi, S. Watanabe, H. Takahashi ", Nucl. Inst. Meth. Phys. Res. B, 153 (1999), 142.

[Sakaguchi, 2004] N. Sakaguchi, S. Watanabe, H. Takahashi, R.G. Faulkner, J. Nucl. Mater., 329-333 (2004), 1166.

[Sakaguchi, 2005] N. Sakaguchi, H. Takahashi, H. Ichinose, Materials Transaction, 46 (2005), 440.

[Watanabe, 1995] S. Watanabe, N. Sakaguchi, N. Hashimoto, H. Takahashi, J. Nucl. Mater., 224 (1995), 158.

[Watanabe, 2000] S. Watanabe, Y. Takamatsu, N. Sakaguchi, H. Takahashi, J. Nucl. Mater., 283-287 (2000), 152.